



# Optical design of multilayer antireflection coatings for indoor solar cell applications

SHIGERU KUBOTA,\* BASHIR AHMMAD, AND FUMIHIKO HIROSE

Graduate School of Science and Engineering, Yamagata University, 4-3-16 Jonan, Yonezawa, Yamagata 992-8510, Japan

\*kubota@yz.yamagata-u.ac.jp

Received 18 November 2022; revised 9 February 2023; accepted 9 February 2023; posted 13 February 2023; published 8 March 2023

Multilayer antireflection coatings (ARCs) for solar cells are conventionally designed to enhance the photocurrent level obtained at normal incidence. This is mainly because outdoor solar panels are usually placed such that they can receive strong midday sunlight at a nearly vertical angle. However, in the case of indoor photovoltaic devices, the direction of light changes considerably with changes in the relative position and angle between the device and light sources; therefore, it is often difficult to predict the incident angle. In this study, we explore a method to design ARCs suitable for indoor photovoltaics by essentially taking into account the indoor lighting environment, which is different from the outdoor conditions. We propose an optimization-based design strategy that aims to enhance the average level of the photocurrent generated when a solar cell receives irradiance randomly from all directions. We apply the proposed method to design an ARC for organic photovoltaics, which are expected to be promising indoor devices, and numerically compare the resultant performance with that obtained using a conventional design method. The results demonstrate that our design strategy is effective for achieving excellent omnidirectional antireflection performance and allows the realization of practical and efficient ARCs for indoor devices. © 2023 Optica Publishing Group

<https://doi.org/10.1364/AO.481123>

## 1. INTRODUCTION

The recent rapid development of the Internet of Things (IoT) (e.g., sensors and remote control) has generated great demand and interest for indoor photovoltaics, because they are easier to handle than batteries, which require periodic replacement [1–3]. Among various photovoltaic technologies, organic photovoltaics (OPVs) possess many desirable properties such as low cost, light weight, flexibility, semitransparency, and nontoxicity [4–6]. In addition, OPVs exhibit excellent indoor performance because of their high fill factor at low light intensities and their absorption wavelength matching the indoor light spectrum [7–11]. Actually, the efficiency of OPVs has been shown to be significantly higher than that of commercial silicon solar cells in a realistic indoor environment [11]. For further improving the efficiency of OPVs, a key limitation is the low mobility of charge carriers in organic semiconductors [12–14]. To facilitate carrier extraction from them, the active layer should be very thin (typically  $\sim 100$  nm), which hinders sufficient absorption of the incident light. Therefore, it is important to develop efficient antireflection (AR) techniques that can reduce surface reflection to enhance absorption in the thin active layer.

Generally, antireflection coatings (ARCs) for solar cells are designed to increase the photocurrent level generated when the solar cell receives light at normal incidence [15]. This conventional design method is attributed to the fact that the outdoor

solar panels are typically placed such that the sunlight with its largest intensity at midday illuminates the panel surface at a near-vertical angle. However, in the case of indoor solar cells, the incident angle varies widely depending on the relative position of the light sources, as well as the direction of the solar cell surfaces. Thus, it is usually difficult to predict the direction of the incident light for indoor devices. Additionally, in an indoor environment, a large portion of the optical energy consists of diffuse light that occurs through multiple reflections at the floor and walls [11]. This is quite different from the outdoor environment, where the main component of the optical energy is direct light from the sun. If we essentially consider the indoor lighting conditions, which differ from the outdoor ones, we could improve the performance of the ARCs for indoor photovoltaic devices.

In this study, we propose a method for designing multilayer ARCs suitable for indoor solar cell applications. In this method, the layer configuration of ARCs is optimized to enhance the average photocurrent level under isotropic lighting conditions, where the solar cell receives irradiance randomly from all directions. We apply the proposed method to design an ARC for an OPV cell and analyze the resultant incident angle-dependent AR properties. We also compare the AR performance obtained by the proposed and conventional design methods, and show that the proposed method plays a role in significantly improving the performance, particularly at large incident angles.

The results offer a practical and useful method to enhance the efficiency of indoor photovoltaic devices.

## 2. METHODS

### A. Optical Modeling

Numerical simulations were conducted to investigate the optical properties of an OPV cell incorporated with  $N$  thin-film AR layers [Fig. 1(a)]. The model of the OPV cell includes a 100 nm thick film of poly(3-hexylthiophene) (P3HT) and [6,6]-phenyl-C<sub>61</sub>-butyric acid methyl ester (PCBM) blend as an active layer, and a 7 nm thick MoO<sub>3</sub> film as a hole transporting layer [16–18]. These films are sandwiched between a 150 nm indium-doped tin oxide layer and 100 nm Al layer, which are the front and back electrodes, respectively. The OPV cell is assumed to be deposited on a 0.7 mm thick glass substrate. The optical parameters (i.e., refractive index and extinction coefficient) of the materials in the OPV cell and glass substrate were obtained by the measurement of spectroscopic ellipsometry. The refractive index of each AR layer is assumed to be an arbitrary value between 1.05 and 2.66 (the extinction coefficient is 0), which is constant for all wavelengths [19,20]. This assumption is adopted to elucidate the theoretically achievable AR performance obtained with arbitrary refractive index values and nearly corresponds to the case where the refractive index can be controlled using nanoporous materials [21]. The thickness of each AR layer is limited between 0 and 400 nm.

To evaluate the performance of the OPV cell, the short-circuit current density ( $J_{SC}$ ) was calculated using characteristic matrix-based analysis, as described in our previous studies [16–18]. Briefly, in this analysis, the optical model consists of

two thin-film stacks, which correspond to the AR layers and OPV cell, and a much thicker glass substrate [Fig. 1(a)]. Within each thin-film stack, light is added coherently according to the theory of the characteristic matrix method [15], whereas, in the thick substrate, the addition of optical irradiances (not electric field amplitudes) is considered because of the loss of coherence. Considering the multiple reflections at the interfaces between the substrate and the two thin-film stacks, the absorbance in the active layer  $A_{act}$  can be obtained by calculating the potential transmittance in the thin-film assembly [15]. In the case of oblique incidence, to treat the input as unpolarized light, the averaging of the optical response obtained with the  $s$ - and  $p$ -polarized light is additionally performed [22].

When the OPV cell receives light with incident angle  $\theta$ , the level of photocurrent  $J_{SC}(\theta)$  is obtained as follows [16–18]:

$$J_{SC}(\theta) = \int_0^{\lambda_g} q_e N_p(\lambda, \theta) F_{NR}(\lambda) d\lambda, \quad (1)$$

where

$$N_p(\lambda, \theta) = A_{act}(\lambda, \theta) F(\lambda) \frac{\lambda}{hc}. \quad (2)$$

Here  $\lambda_g$  is the wavelength corresponding to the bandgap of P3HT (653 nm) (Fig. 2, dashed lines), and  $q_e$  is the elementary charge.  $N_p(\lambda, \theta)$  and  $A_{act}(\lambda, \theta)$  are the number of absorbed photons and the absorbance in the active layer, respectively, at wavelength  $\lambda$  and incident angle  $\theta$ .  $F_{NR}(\lambda)$  is the non-recombination factor, which is simply assumed to be  $F_{NR}(\lambda) = 1$  at all values of  $\lambda$  [23].  $h$  is Planck's constant, and  $c$  is the speed of light in free space.  $F(\lambda)$  is the irradiance spectrum of the incident light, which is assumed to be the spectrum of sunlight (AM1.5 standard) [24], LED [7], or fluorescent lamp (FL) [25] (Fig. 2).

### B. Optimization

To explore the ARC design suitable for indoor photovoltaics, we optimized the layer configuration (i.e., the refractive index and thickness) of the ARC for the OPV cell [Fig. 1(a)]. In indoor conditions, the direction of the incident light varies widely depending on the relative position and angle between the solar cell and light sources, as mentioned above. Therefore, at the timing when the ARC is designed, it will be generally quite difficult to predict the direction of the incident light. This is particularly the case when we consider the ARC design for mobile devices (e.g., active RFID tags and wearable IoT devices) or for solar cells that can be used in common for various purposes (e.g., different types of sensors). In addition, a substantial portion of the optical energy in an indoor environment is attributed to diffuse light, which occurs through reflection at the surfaces of various objects, walls, and floor, and then hits the solar cells from everywhere [11]. Therefore, in many design cases, it is a natural and reasonable assumption that indoor devices receive optical energy randomly from any angle or receive isotropic light, as illustrated in Fig. 1(b).

With this isotropic lighting assumption, the irradiance  $dE$  that a solar cell receives by the light ray contained in an elementary solid angle  $d\Omega$ , corresponding to incident angle  $\theta$ , is described as follows [11,26]:

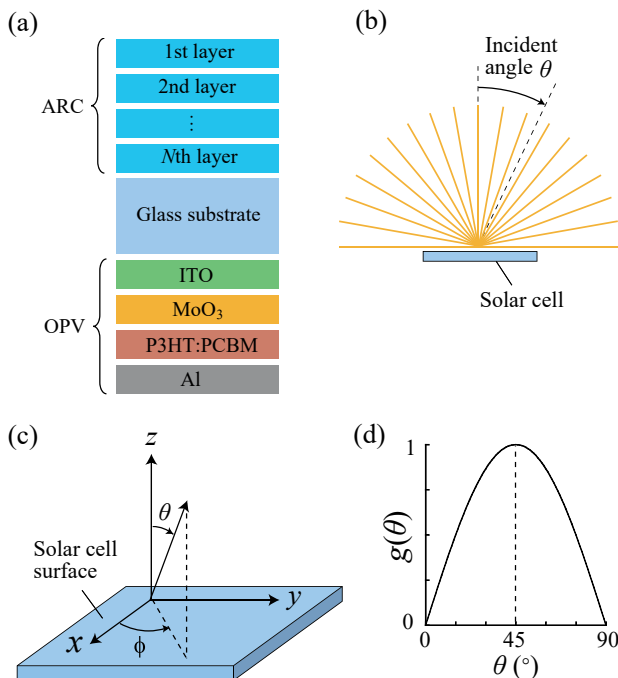


**Fig. 1.** (a) Optical model of the OPV cell with the ARC. (b) Schematic diagram representing the isotropic lighting condition under which a solar cell receives light from all directions. (c) Definition of spherical coordinates ( $\theta$ ,  $\phi$ ). (d) Density function  $g(\theta)$  of irradiance under the isotropic lighting condition [Eq. (6)].

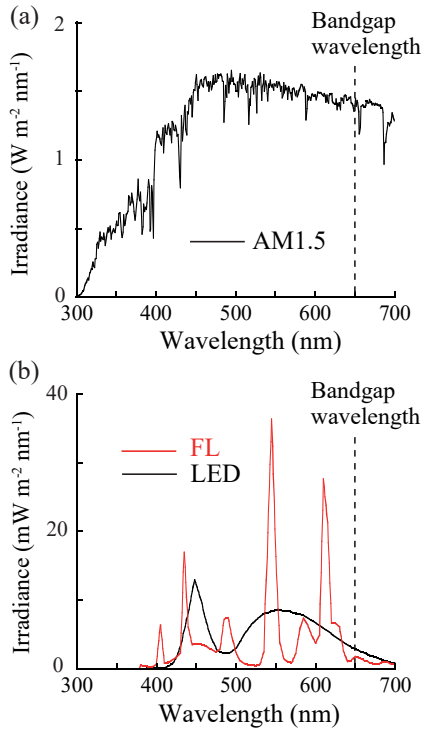


**Fig. 2.** (a) Irradiance spectra for the sunlight (AM1.5). (b) LED (black) and FL (red). The vertical dashed lines show the wavelength corresponding to the bandgap energy of P3HT (653 nm).

$$dE = L(\lambda) \cos(\theta) d\Omega. \quad (3)$$

In this equation,  $L(\lambda)$  is the radiance, which depends only on the wavelength  $\lambda$  (and not on the incident angle  $\theta$ , from our assumption). By introducing spherical coordinates  $(\theta, \phi)$ , as shown in Fig. 1(c), the solid angle in Eq. (3) can be rewritten as

$$d\Omega = \sin(\theta) d\theta d\phi. \quad (4)$$

Here let us define  $g(\theta)$  as the density function (or probability density function) of irradiance for each value of  $\theta$ , which satisfies the constraint  $\int_0^{\pi/2} g(\theta) d\theta = 1$ . Then the irradiance of light, corresponding to the incident angle between  $\theta$  and  $\theta + d\theta$ , can be described by using an integral of the right-hand side of Eq. (3) with respect to  $\phi$  as follows:

$$F(\lambda)g(\theta)d\theta = L(\lambda) \sin(\theta) \cos(\theta) d\theta \int_0^{2\pi} d\phi, \quad (5)$$

with the irradiance spectrum  $F(\lambda)$  [Eq. (2)]. By applying the above-mentioned constraint of  $g(\theta)$  to Eq. (5), we find  $F(\lambda) = \pi L(\lambda)$ . Therefore, by using Eq. (5) again,  $g(\theta)$  is described as follows:

$$g(\theta) = \sin(2\theta). \quad (6)$$

The shape of the function  $g(\theta)$ , shown in Fig. 1(d), suggests that the irradiance density is symmetric with respect to  $\theta = 45^\circ$ , which gives the highest level and goes to zero as  $\theta$  deviates from this angle. Importantly, this result implies that the conventional design strategy, which aims to increase the photocurrent level at  $\theta = 0^\circ$  (i.e., normal incidence) [15], might not be the most suitable for indoor ARCs.

Therefore, alternatively, we propose to design ARCs that can enhance the average photocurrent level under the isotropic lighting condition, which is described as

$$J_{SC,ave} = \int_0^{\pi/2} J_{SC}(\theta)g(\theta)d\theta. \quad (7)$$

Note that  $J_{SC,ave}$  is the expected value of  $J_{SC}$  when the direction of light is not predictable; therefore, based on the isotropic lighting assumption, it is statistically valid to maximize this value to improve the indoor solar cell efficiency. Therefore, we propose an optimization design method for ARCs in which  $J_{SC,ave}$  is used as the objective function, and we refer to this method as Method A. In addition, for comparison, we also use a conventional design method in which  $J_{SC}(0)$  (i.e., the value of  $J_{SC}$  at  $\theta = 0^\circ$ ) is used as the objective function, and we refer to this method as Method B.

Throughout the current study, during the optimization search, the objective function values were evaluated using the AM1.5 solar spectrum. This is because the solar spectrum is broader and contains irradiance at shorter wavelengths ( $<400$  nm), which are not included in the spectrum of indoor light sources (Fig. 2). Generally, in an indoor environment, the optical energy results not only from indoor illumination, but also from sunlight entering through windows. Thus, to consider the entire wavelength range of interest in the optimization process and obtain a broadband AR function, it is adequate to use the solar spectrum for the objective function.

For optimization with both Methods A and B, we applied the multistart algorithm [27] to search for the refractive index and thickness of the AR layers, which give the largest value of the objective function. In the multistart algorithm, local searches using the quasi-Newton method [28] are performed repetitively from random initial points (1000 points for each simulation case) to find a global optimal solution. The computation time required for searching a global optimal solution for a four-layer ARC, for example, is 55 and 0.81 h for Methods A and B, respectively, by using an Intel Xeon E5-2660 v4 personal computer (2.00 GHz) and a program written in C++. This implies that the proposed method takes  $\sim 70$  times longer time than the conventional method. This difference can be partly explained by the fact that, for calculating the integral term in Eq. (7) with sufficient accuracy, the domain of  $\theta$  (i.e., from  $0^\circ$  to  $90^\circ$ ) is discretized with intervals of  $2^\circ$  in the proposed method.

### 3. RESULTS AND DISCUSSION

To examine the effectiveness of the proposed method for designing indoor ARCs, we numerically analyzed the change in the photocurrent level of OPVs corresponding to a change in the configuration of the ARCs. The proposed design strategy of Method A, which maximizes the objective function  $J_{SC,ave}$ , could lead to a relative decrease in the value of  $J_{SC}(0)$ , which is the objective function used in the conventional design strategy of Method B. Conversely, the application of Method B, which maximizes  $J_{SC}(0)$ , could lead to a relative decrease in  $J_{SC,ave}$ . To clarify this trade-off relationship, we evaluated, as shown in Fig. 3, the four values of the photocurrent,  $J_{SC,ave}^X$  and  $J_{SC,0}^X$  (with  $X = A$  and B), which are defined as follows:

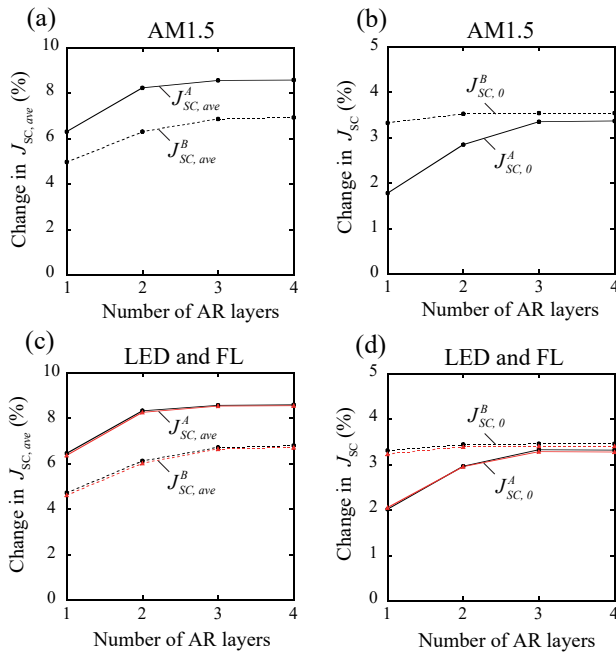


**Fig. 3.** Change in the values of (a) and (c)  $J_{SC,ave}^A$  and  $J_{SC,ave}^B$ , and (b) and (d)  $J_{SC,0}^A$  and  $J_{SC,0}^B$  as a function of the number of AR layers. The spectrum of the incident light is that of the (a) and (b) AM1.5 standard, and (c) and (d) LED (black) and FL (red). The  $y$  coordinate is the relative change in (a) and (c)  $J_{SC,ave}$  (b) or (d)  $J_{SC}(0)$  from the corresponding value obtained without the ARC. The solid and dashed lines are used for the cases where the ARC is designed with Methods A and B, respectively.

- (1)  $J_{SC,ave}^A$  is the value of  $J_{SC,ave}$  optimized with Method A,
- (2)  $J_{SC,0}^B$  is the value of  $J_{SC}(0)$  optimized with Method B,
- (3)  $J_{SC,0}^A$  is the value of  $J_{SC}(0)$  obtained by applying the ARC which is optimized with Method A,
- (4)  $J_{SC,ave}^B$  is the value of  $J_{SC,ave}$  obtained by applying the ARC which is optimized with Method B.

Obviously, the values of  $J_{SC,ave}^A$  and  $J_{SC,0}^B$  are the optimal values for  $J_{SC,ave}$  and  $J_{SC}(0)$ , respectively. In contrast,  $J_{SC,ave}^B$  and  $J_{SC,0}^A$  are not the optimal values of  $J_{SC,ave}$  and  $J_{SC}(0)$  because they are obtained as a result of the optimization for  $J_{SC}(0)$  and  $J_{SC,ave}$ , respectively.

Figures 3(a) and 3(b) show the change in these four values under the AM1.5 spectrum when the number of AR layers ( $N$ ) is altered. As expected from the definition of these values,  $J_{SC,ave}^A$  and  $J_{SC,0}^B$  are larger than  $J_{SC,ave}^B$  and  $J_{SC,0}^A$ , respectively, for all the cases shown in the figures. However, as  $N$  increases, the difference between  $J_{SC,0}^A$  and  $J_{SC,0}^B$  becomes very small [Fig. 3(b)], whereas the difference between  $J_{SC,ave}^A$  and  $J_{SC,ave}^B$  is kept at a greater level [Fig. 3(a)]. [Note the difference in vertical scales between Figs. 3(a) and 3(b)]. In addition, all lines in Figs. 3(a) and 3(b) are almost saturated at larger  $N$  values ( $N \geq 3$ ), implying that the results for large  $N$  approximately give the maximum levels of  $J_{SC,ave}^X$  and  $J_{SC,0}^X$  ( $X = A$  and  $B$ ) which can be achieved by each method. Therefore, from the results for  $N = 4$ , we can consider that the achievable level of  $J_{SC,ave}^A$  is significantly (1.53%) higher than that of  $J_{SC,ave}^B$  [Fig. 3(a)], whereas the

difference in the achievable levels of  $J_{SC,0}^A$  and  $J_{SC,0}^B$  (0.17%) is very small [Fig. 3(b)]. This finding importantly suggests that the proposed method is significantly more effective in improving the average photovoltaic efficiency under the indoor isotropic lighting condition than the conventional method, while maintaining the efficiency for the normal incidence condition at a level comparable to that obtained with the conventional method. In addition, in Figs. 3(c) and 3(d), we performed the same simulations as those in Figs. 3(a) and 3(b), except that the light source is changed into LED and FL. The results obtained were quite similar for both outdoor and indoor light sources. This can be partly explained from the fact that the AR effect arises in a broad wavelength range, which contains the spectral region where outdoor and indoor lights have strong intensity (Fig. 2) [also see Fig. 5]. The results additionally suggest that the effectiveness of the proposed method is robust against changes in the irradiance spectrum of light. This robustness is beneficial because, in an indoor environment, the irradiance spectrum is modulated variously owing to the effects of reflection and absorption by various things, which depend on the position in a room [30].

We also compared the optimal values of the refractive index and thickness of the AR layers, which are obtained using both design methods. As shown in Table 1, we found that, for the ARC designed by the proposed method, there is a tendency for the optimal values of the refractive index to become slightly ( $\leq 0.10$ ) lower and those of the layer thickness to become higher to some degree (by 8.7–160.0 nm), compared with the values of the ARC designed by the conventional method. The refractive index values obtained by both methods gradually increase from the front side to the rear side, which are similar to the results of previous studies [31–33]. In addition, the total thickness of the ARCs obtained by both methods is quite small ( $< 610$  nm), implying that they are applicable to flexible devices such as OPVs [34].

Additionally, in Fig. 4, we analyzed the incident angle-dependent change in  $J_{SC}$  in cases where the four-layer ARC, which is designed with either Method A or B, is applied to the OPV cell. The results showed that, regardless of whether the outdoor [Fig. 4(a)] or indoor [Figs. 4(b) and 4(c)] light sources are used, the  $J_{SC}$  value at a small incident angle ( $\theta < 55^\circ$ ) increases to nearly the same level by applying the ARCs designed with the two methods [also see Fig. 4(d) for the comparison of Figs. 4(a)–4(c)]. This result is consistent with the previous one [Figs. 3(b) and 3(d)], which states that the difference between  $J_{SC,0}^A$  and  $J_{SC,0}^B$  is very small for large  $N$ . On the other hand, as shown in Figs. 4(a)–4(c), the increase in the level of  $J_{SC}$  at a large incident angle ( $\theta > 55^\circ$ ) is substantially higher for the ARC designed with Method A (red lines) than for the ARC designed with Method B (blue lines). The results presented here indicate that the proposed method significantly enhances the photocurrent at large angles while maintaining nearly the same level of photocurrent at small angles as that obtained by the conventional method. This finding was further clarified by examining the change in the spectrum of reflectance and that of absorbance in the active layer, which is caused by applying the ARCs. The results in Fig. 5 show that, regardless of the  $\theta$  values, the reflectance decreases and the absorbance increases over a broad wavelength range (from 300 to 700 nm) by applying the

**Table 1. Examples of the Optimal Values of the Refractive Index and Thickness of the AR Layers Obtained by the Proposed Method (Method A) and the Conventional Method (Method B)<sup>a</sup>**

Layer	N = 2			N = 4		
	Method A	Method B	Difference	Method A	Method B	Difference
1st	$n = 1.05$ (263.9)	$n = 1.11$ (103.9)	-0.06 (+160.0)	$n = 1.05$ (240.9)	$n = 1.06$ (105.5)	-0.01 (+135.4)
2nd	$n = 1.24$ (123.9)	$n = 1.34$ (85.4)	-0.10 (+38.5)	$n = 1.16$ (121.0)	$n = 1.22$ (92.5)	-0.06 (+28.5)
3rd	-	-	-	$n = 1.37$ (90.0)	$n = 1.41$ (81.3)	-0.04 (+8.7)
4th	-	-	-	$n = 1.54$ (157.5)	-	-

<sup>a</sup>Each row shows the values of the refractive index ( $n$ ) and thickness (in nm) (in parentheses) for each layer of the ARC, when the total number of AR layers,  $N$ , is 2 and 4. The results obtained with Methods A and B as well as the difference between them (i.e., (the value with Method A) - (the value with Method B)) are shown together. The ‘-’ mark for the case of  $N = 4$  and Method B means that the thickness of the 4th layer has converged to zero as a result of optimization, implying that a 3-layer ARC is sufficient to increase the objective function value for this case.

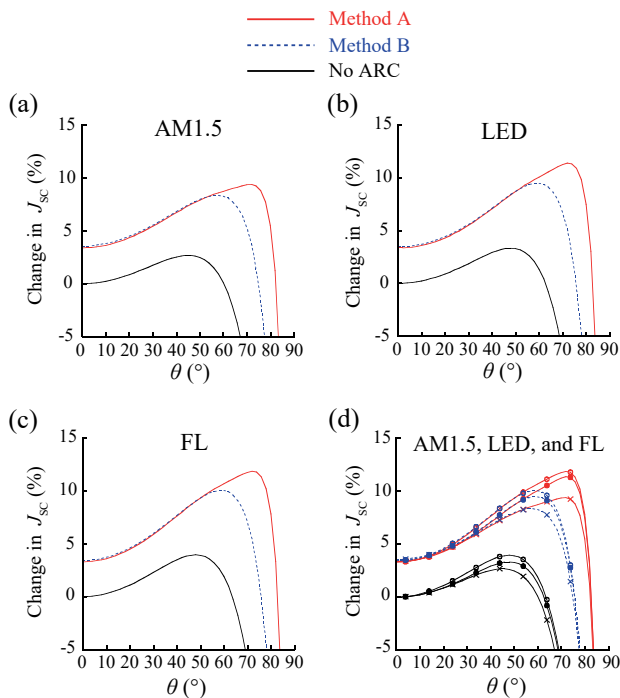


**Fig. 4.** Dependence of  $J_{sc}$  on the incident angle  $\theta$ . (a), (b), and (c) show the cases of illumination with the AM1.5, LED, and FL spectra, respectively. (d) shows the plot of (a)–(c) together. In (a)–(d), the  $y$  coordinate is the relative change in  $J_{sc}$  from the reference value, which is the value of  $J_{sc}$  obtained at  $\theta = 0^\circ$  without the ARC. The black lines show the cases without the ARC, and the color lines show the cases with the four-layer ARC designed with either Method A (red) or B (blue). In (d), the  $x$  marks, closed circles, and open circles correspond to the cases using light with the AM1.5, LED, and FL spectra, respectively.

ARCs obtained with both design methods. Additionally, for small  $\theta$  ( $\theta = 0^\circ$  and  $45^\circ$ ), the reflectance and absorbance spectra are nearly the same regardless of whether the ARC is designed with Method A or B [Figs. 5(a)–5(d)]. On the other hand, for larger  $\theta$  ( $\theta = 75^\circ$  and  $82.5^\circ$ ), the reflectance significantly decreases, whereas the absorbance significantly increases, by applying the ARC designed with Method A, as compared to that designed with Method B [Figs. 5(e)–5(h)]. This result indicates a large difference in the reflection and absorption properties depending on the design method only at large incident angles, which supports the previous result shown in Fig. 4. The results

obtained so far consistently indicate that the proposed ARC design method is quite effective not only for achieving excellent indoor performance under isotropic light conditions, but also for improving large-angle performance.

**4. CONCLUSION**

In cases where we aim to design an ARC for application to indoor solar cells, it will be difficult in many situations to predict the direction of incident light at the time of the design process. In such situations, it is often reasonable to make an assumption that the solar cell receives irradiance randomly from all directions, which we call the isotropic lighting assumption. In this study, we propose a method for designing ARCs, in which the layer configuration is optimized to increase the expected value of  $J_{sc}$  generated under isotropic light. The optical properties of the ARC designed using the proposed method were compared with those designed using the conventional method, which intends to increase the photocurrent induced at normal incidence. We showed that the average level of  $J_{sc}$  under the isotropic lighting condition is significantly increased by the proposed method compared to the conventional method and, furthermore, that the ARC provided by the proposed method has the advantage of allowing excellent omnidirectional performance. However, it should be mentioned that the proposed design method has the disadvantage of requiring a much longer time to search for optimal solutions (as described in the methods). Our method is based on the assumption of a somewhat complicated lighting environment, which is mathematically described by the density function  $g(\theta)$  for irradiance [Eq. (6)]. In other words, the proposed method improves the performance under the indoor conditions, instead of increasing the computational cost to numerically reproduce the corresponding lighting environment.

There are several past studies on the optical design of ARCs that have utilized optimization under the condition of not normal incidence, as in our study. Two simulation studies [20,35] proposed a method based on the optimization of the temporal average of the incident quantum efficiency [20] or photocurrent level [35], which is estimated from detailed data on the time-dependent direction and strength of sunlight at specific locations. A numerical and experimental study [32], which dealt with the ARC with nanoporous materials, used the optimization of a simple average of reflectance over both wavelengths and incident angles. Our study and these previous studies are based

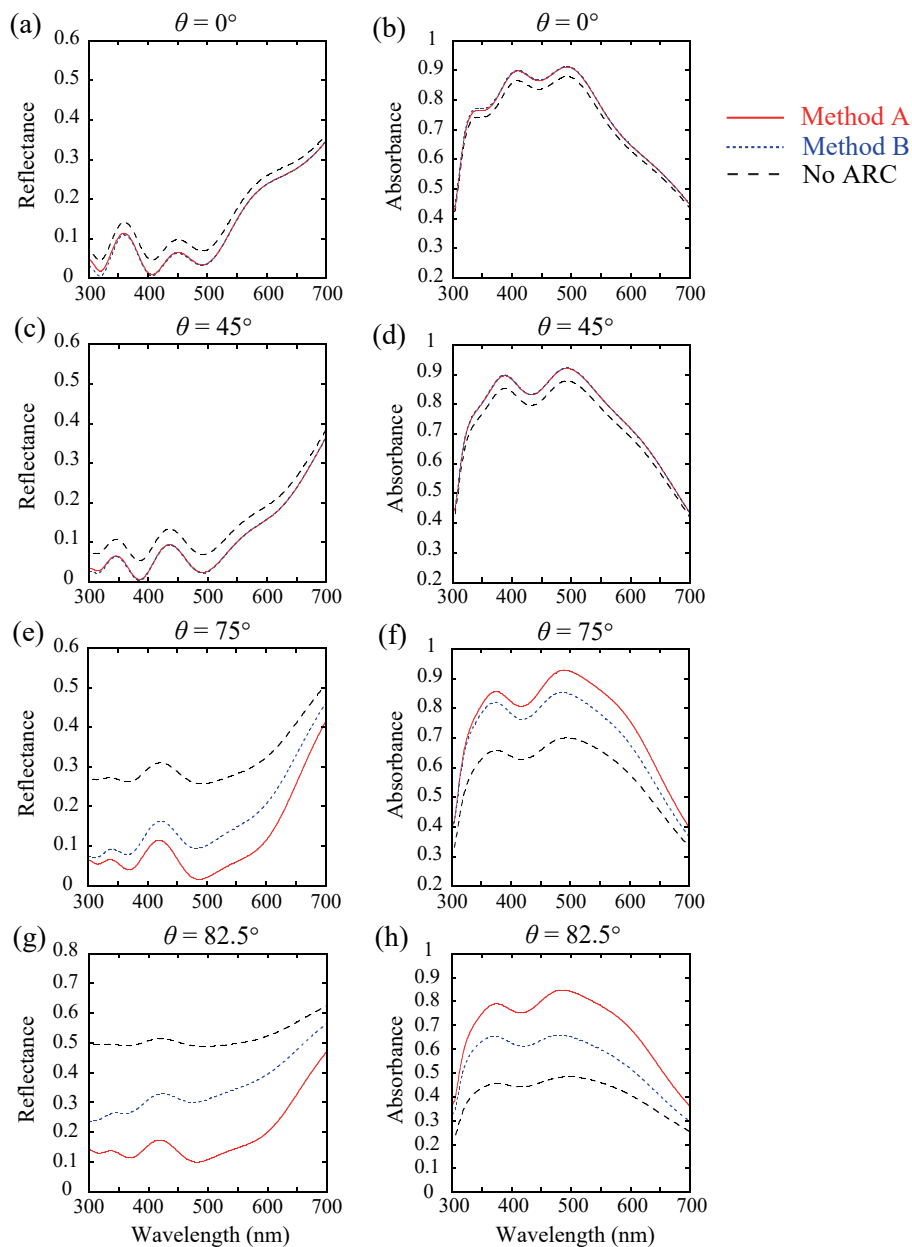


**Fig. 5.** Spectra of the reflectance (left column) and the absorbance in the active layer (right column) for an incident angle (a) and (b) of  $0^\circ$ , (c) and (d)  $45^\circ$ , (e) and (f)  $75^\circ$ , and (g) and (h)  $82.5^\circ$ . In (a)–(h), the black lines represent the cases without the ARC, and the color lines represent the cases with the four-layer ARC, which is designed with either Method A (red) or B (blue). The wavelength range (300–700 nm) is selected to include the region from the shortest wavelength of the indoor and outdoor light to the bandgap wavelength of P3HT (653 nm) (Fig. 2), which is associated with photocurrent generation. The increase in reflectance and the decrease in absorbance at a longer wavelength, which is similar to previous studies [18,29], is attributable to the fact that it is difficult for the organic semiconductor material to absorb sufficient light around the bandgap wavelength.

on a similar design framework, in which an objective function containing a relatively large amount of information, is used for optimization to achieve higher performance at the expense of computational cost. This design framework is promising for realizing efficient AR functions that are particularly suitable for specific purposes (for example, for indoor use in our study) and can be extended to design ARCs for various types of photovoltaic technologies. A worthwhile future study will be to more

comprehensively elucidate the change in the performance associated with the change in the objective function under various lighting environments for different photovoltaic devices.

**Funding.** Japan Society for the Promotion of Science (JSPS) KAKENHI (21K04825).

**Disclosures.** The authors declare no conflicts of interest.

**Data availability.** Data underlying the results presented in this paper are not publicly available at this time but may be obtained from the authors upon reasonable request.

## REFERENCES

1. M. A. Alkhalayfeh, A. A. Aziz, M. Z. Pakhuruddin, K. M. M. Katubi, and N. Ahmadi, "Recent development of indoor organic photovoltaics," *Phys. Status Solidi A* **219**, 2100639 (2022).
2. L. Xie, W. Song, J. Ge, B. Tang, X. Zhang, T. Wu, and Z. Ge, "Recent progress of organic photovoltaics for indoor energy harvesting," *Nano Energy* **82**, 105770 (2021).
3. S. S. Yang, Z. C. Hsieh, M. L. Keshotov, G. D. Sharma, and F. C. Chen, "Toward high-performance polymer photovoltaic devices for low-power indoor applications," *Sol. RRL* **1**, 1700174 (2017).
4. Y. Wang, P. Shen, J. Liu, Y. Xue, Y. Wang, M. Yao, and L. Shen, "Recent advances of organic solar cells with optical microcavities," *Sol. RRL* **3**, 1900181 (2019).
5. K. A. Mazzi and C. K. Luscombe, "The future of organic photovoltaics," *Chem. Soc. Rev.* **44**, 78–90 (2015).
6. N. Schopp and V. V. Brus, "A review on the materials science and device physics of semitransparent organic photovoltaics," *Energies* **15**, 4639 (2022).
7. B. Minnaert and P. Veelaert, "A proposal for typical artificial light sources for the characterization of indoor photovoltaic applications," *Energies* **7**, 1500–1516 (2014).
8. B. Minnaert and P. Veelaert, "The appropriateness of organic solar cells for indoor lighting conditions," *Proc. SPIE* **7722**, 77221P (2010).
9. R. Steim, T. Ameri, P. Schilinsky, C. Waldauf, G. Dennler, M. Scharber, and C. J. Brabec, "Organic photovoltaics for low light applications," *Sol. Energy Mater. Sol. Cells* **95**, 3256–3261 (2011).
10. J. Bachmann, C. Buerhop-Lutz, R. Steim, P. Schilinsky, J. A. Hauch, E. Zeira, and B. J. Christoh, "Highly sensitive non-contact shunt detection of organic photovoltaic modules," *Sol. Energy Mater. Sol. Cells* **101**, 176–179 (2012).
11. C. A. Reynaud, R. Clerc, P. B. Lechene, M. Hebert, A. Cazier, and A. C. Arias, "Evaluation of indoor photovoltaic power production under directional and diffuse lighting conditions," *Sol. Energy Mater. Sol. Cells* **200**, 110010 (2019).
12. M. Niggemann, B. Blasi, A. Gombert, A. Hinsch, H. Hoppe, P. Lalanne, D. Meissner, and V. Wittwer, "Trapping light in organic plastic solar cells with integrated diffraction gratings," in *Proc. 17th Eur. Photovoltaic Solar Energy Conf.* (2001).
13. M. Niggemann, M. Riede, A. Gombert, and K. Leo, "Light trapping in organic solar cells," *Phys. Status Solidi A* **205**, 2862–2874 (2008).
14. A. Raman, Z. Yu, and S. Fan, "Dielectric nanostructures for broadband light trapping in organic solar cells," *Opt. Express* **19**, 19015–19026 (2011).
15. H. A. Macleod, *Thin-Film Optical Filters*, 4th ed. (CRC Press, 2010).
16. S. Kubota, Y. Harada, T. Sudo, K. Kanomata, B. Ahmmad, J. Mizuno, and F. Hirose, "An integrated antireflection design using nanotexture and high-refractive-index glass for organic photovoltaics," *J. Coat. Technol. Res.* **14**, 1209–1224 (2017).
17. S. Kubota, K. Kanomata, B. Ahmmad, J. Mizuno, and F. Hirose, "Optimized design of moth eye antireflection structure for organic photovoltaics," *J. Coat. Technol. Res.* **13**, 201–210 (2016).
18. S. Kubota, K. Kanomata, K. Momiyama, T. Suzuki, and F. Hirose, "Robust design method of multilayer antireflection coating for organic solar cells," *IEICE Trans. Electron.* **96**, 604–611 (2013).
19. Y. J. Chang and Y. T. Chen, "Broadband omnidirectional antireflection coatings for metal-backed solar cells optimized using simulated annealing algorithm incorporated with solar spectrum," *Opt. Express* **19**, A875–A887 (2011).
20. X. Guo, Q. Liu, H. Tian, B. Li, H. Zhou, C. Li, A. Hu, and X. He, "Optimization of broadband omnidirectional antireflection coatings for solar cells," *J. Semicond.* **40**, 032702 (2019).
21. J. Q. Xi, M. F. Schubert, J. K. Kim, E. F. Schubert, M. Chen, S. Y. Lin, W. Liu, and J. A. Smart, "Optical thin-film materials with low refractive index for broadband elimination of Fresnel reflection," *Nat. Photonics* **1**, 176–179 (2007).
22. W. Ren, G. Zhang, Y. Wu, H. Ding, Q. Shen, K. Zhang, J. Li, N. Pan, and X. Wang, "Broadband absorption enhancement achieved by optical layer mediated plasmonic solar cell," *Opt. Express* **19**, 26536–26550 (2011).
23. A. Y. Darkwi, W. K. Lote, and K. Ibrahim, "Computer simulation of collection efficiency of a-Si:H tandem solar cells interconnected by transparent conductive oxide," *Sol. Energy Mater. Sol. Cells* **60**, 1–9 (2000).
24. "Standard tables for reference solar spectral irradiances," ASTM G173-03 (ASTM International, 2005).
25. "Colorimetry," CIE 15:2004 (International Commission on Illumination, 2004), 3rd ed.
26. M. Born and E. Wolf, *Principles of Optics: Electromagnetic Theory of Propagation, Interference and Diffraction of Light*, 7th ed. (Cambridge University, 1999).
27. A. H. G. R. Kan and G. T. Timmer, "Stochastic global optimization methods. Part 1: Clustering methods," *Math. Program.* **39**, 27–56 (1987).
28. W. H. Press, S. A. Teukolsky, W. T. Vetterling, and B. P. Flannery, *Numerical Recipes: The Art of Scientific Computing*, 3rd ed. (Cambridge University, 2007).
29. K. Forberich, G. Dennler, M. C. Scharber, K. Hingerl, T. Fromherz, and C. J. Brabec, "Performance improvement of organic solar cells with moth eye anti-reflection coating," *Thin Solid Films* **516**, 7167–7170 (2008).
30. G. Apostolou, A. Reinders, and M. Verwaal, "Comparison of the indoor performance of 12 commercial PV products by a simple model," *Energy Sci. Eng.* **4**, 69–85 (2016).
31. M. Chen, H. C. Chang, A. S. P. Chang, S. Y. Lin, J. Q. Xi, and E. F. Schubert, "Design of optical path for wide-angle gradient-index antireflection coatings," *Appl. Opt.* **46**, 6533–6538 (2007).
32. D. J. Poxson, M. F. Schubert, F. W. Mont, E. F. Schubert, and J. K. Kim, "Broadband omnidirectional antireflection coatings optimized by genetic algorithm," *Opt. Lett.* **34**, 728–730 (2009).
33. E. Osorio, R. Urteaga, L. N. Acquaroli, G. Garcia-Salgado, H. Juarez, and R. R. Koropecski, "Optimization of porous silicon multilayer as antireflection coatings for solar cells," *Sol. Energy Mater. Sol. Cells* **95**, 3069–3073 (2011).
34. G. Perrakis, A. C. Tasolamprou, G. Kenanakis, E. N. Economou, S. Tzortzakis, and M. Kafesaki, "Submicron organic-inorganic hybrid radiative cooling coatings for stable, ultrathin, and lightweight solar cells," *ACS Photonics* **9**, 1327–1337 (2022).
35. S. A. Boden and D. M. Bagnall, "Sunrise to sunset optimization of thin film antireflective coatings for encapsulated, planar silicon solar cells," *Prog. Photovoltaics* **17**, 241–252 (2009).